Original article

Title: Genetic factors derived from the MRL/MpJ mouse function to maintain the integrity of spermatogenesis after heat exposure

Authors: Masataka CHIHARA,* Teppei NAKAMURA,*† Saori OTSUKA-KANAZAWA,* Osamu ICHII,* Yaser Hosny Ali ELEWA*‡ and Yasuhiro KON*

Affiliations: Laboratory of Anatomy, Department of Biomedical Sciences, Graduate School of Veterinary Medicine, Hokkaido University, Kita 18, Nishi 9, Kita-ku, Sapporo 060-0818, Japan*

Section of Biological Safety Research, Chitose Laboratory, Japan Food Research Laboratories, 2–3 Bunkyou, Chitose, Hokkaido 066-0052, Japan†

Department of Histology and Cytology, Faculty of Veterinary Medicine, Zagazig University, Zagazig 44519, Egypt‡

Number of text pages: 36

Number of tables: 1

Number of figures: 7

Keywords: heat stress; testis; spermatogenesis; calcification; mouse strain; MRL/MpJ

Corresponding author: Yasuhiro Kon, DVM, PhD, Laboratory of Anatomy, Department of Biomedical Sciences, Graduate School of Veterinary Medicine, Hokkaido University, Kita18-Nishi 9, Kita-ku, Sapporo 060-0818, Japan. Tel/Fax: +81 11 706 5189; E-mail: y-kon@vetmed.hokudai.ac.jp

ABSTRACT

MRL/MpJ mice possess highly heat-shock resistant spermatocytes (HRS) in comparison with C57BL/6 mice. This resistance depends on the MRL/MpJ-type loci at the 81 cM region of Chromosome (Chr) 1 and the 40 cM region of Chr 11. To evaluate the functions of these loci in detail, we examined the histopathological changes resulting from experimental cryptorchidism or transient scrotal heat stress (SHS) in the testes of C57BL/6-based congenic strains (B6.MRLc1, B6.MRLc11, and B6.MRLc1c11) carrying the MRL/MpJ-derived loci responsible for HRS. Among cryptorchid testes from congenic strains, those in B6.MRLc1c11 mice showed the highest heat resistance, indicating that the genetic interactions between MRL/MpJ-derived HRS loci on Chrs 1 and 11 may be important for maintaining spermatogenesis under continuous testicular hyperthermia. In contrast, immediately after SHS induction, germ cell loss via apoptosis was inhibited in B6.MRLc11 and B6.MRLc1c11 mice, similar to that in MRL/MpJ mice. However, this HRS phenotype was not observed in C57BL/6 or B6.MRLc1 mice. Furthermore, testicular calcification due to long-term damage by SHS induction was inhibited in all congenic strains in comparison with that in C57BL/6 mice, indicating that each MRL/MpJ-derived locus on Chrs 1 and 11 acted independently to facilitate the recovery of heat-induced testicular damage by inhibiting calcification. B6.MRLc11 and B6.MRLc1c11 mice showed greater recovery in spermatogenesis than B6.MRLc1 mice 60 days after SHS induction.

Therefore, the MRL/MpJ-derived HRS locus on Chr 11 might play an important role in recovery from heat stress damage. Based on these results, we concluded that MRL/MpJ-derived loci on Chrs 1 and 11 regulate testicular heat sensitivity through different mechanisms.

Introduction

Male germ cells, or sperm, are produced in a cyclic and complex process called spermatogenesis, which occurs within the seminiferous tubules of the testes. Mammalian spermatogenesis is divided into three phases: mitotic proliferation of stem spermatogonia, meiotic differentiation of spermatocytes, and transformation of spermatids into spermatozoa. Germ cell differentiation is regulated and supported by somatic Sertoli cells, which line the seminiferous tubules. In most mammals, the testes are located in the scrotum outside the main abdominal cavity. The temperature within the scrotum is regulated by a specialized blood supply that acts as a heat exchange system. Thus, scrotal temperature is kept lower than the core body temperature (Ivell 2007). Disruption of this system has an adverse effect on spermatogenesis in several species, including humans (Rockett *et al*. 2001; Garolla *et al*. 2013).

Many studies have shown that exposure of the testes to a high-temperature environment (i.e., surgical induction of cryptorchidism or mild testicular heat exposure) damages the seminiferous epithelium, resulting in germ cell loss by apoptosis and alterations in Sertoli cell morphology and function (Yin *et al.* 1997; Lue *et al.* 1999; Guo *et al.* 2007; Li *et al.* 2013). The cells most sensitive to testicular heat stress are spermatocytes (at the leptotene, zygotene, and pachytene stages during meiosis) and round spermatids (Blacksaw *et al.* 1973; Parvinen 1973). Moreover, testicular heat stress impairs protein, DNA, and RNA biosynthesis

(Steinberger 1991), damages spermatocyte DNA, and disrupts chromatin packing in sperm nuclei (Garolla *et al.* 2013; Paul *et al.* 2008). However, the molecular mechanisms responsible for degenerative changes that occur during heat-induced testicular dysfunction remain largely unknown.

We have reported several unique characteristics of the MRL/MpJ mouse testis, such as the appearance of testicular oocytes (Otsuka *et al.* 2008), a lower testis to body weight ratio than that in other inbred strains (Otsuka *et al.* 2010), metaphase-specific apoptosis of meiotic spermatocytes (Kon *et al.* 1999; Kon & Endoh 2000; Namiki *et al.* 2003; Kon 2005), and heat-shock resistant spermatocytes (HRS) (Kon & Endoh 2001; Kazusa *et al.* 2004). In addition, MRL/MpJ mice exhibit regenerative wound healing, such as the closure of ear punches and cardiomyocyte regeneration (Clark *et al.* 1998; Leferovich *et al.* 2001). The presence of these phenotypes depends on the MRL/MpJ genetic background, which is derived from C57BL/6, C3H/He, AKR/J, and LG/J mice (Murphy 1981). Using quantitative trait loci analysis of experimental cryptorchidism, we found that MRL/MpJ-type Chromosomes (Chrs) 1 (81 cM region) and 11 (40 cM region) contained the loci responsible for HRS (Namiki *et al.* 2005). However, we also demonstrated that the locus on MRL/MpJ-type Chr 1 responsible for HRS was insufficient to protect spermatocytes from heat-induced damage (Chihara *et al.* 2014).

Therefore, to clarify the mechanisms regulating testicular heat sensitivity, it is essential to assess the genetic interaction between MRL/MpJ-type HRS loci on Chrs 1 and 11.

In the present study, we investigated the roles of the MRL/MpJ-type loci in testicular heat-resistance by comparing the pathological features of the testis after continuous or transient heat stress induction in C57BL/6, MRL/MpJ mice, and C57BL/6-based congenic mouse strains carrying the MRL/MpJ-type Chrs 1 and/or 11. Although both HRS-related MRL/MpJ-type loci (Chrs 1 and 11) were necessary to maintain spermatogenesis under continuous hyperthermia, the MRL/MpJ-type locus on Chr 11 alone was sufficient to mitigate damage induced by transient hyperthermia. Based on these results, we propose that MRL/MpJ-derived loci on Chrs 1 and 11 regulate testicular heat-resistance through different mechanisms.

Materials and Methods

Animals

C57BL/6 and MRL/MpJ mice were purchased from an animal-breeding company (Japan SLC, Hamamatsu, Japan). The C57BL/6-background congenic mouse strain B6.MRL-(*D1Mit202–D1Mit403*) carrying the telomeric region of MRL/MpJ-type Chr 1 (67.97–81.63 cM) (B6.MRLc1) was generated in our laboratory (Otsuka *et al.* 2010). Similarly, we generated the C57BL/6-background congenic mouse strain

B6.MRL-(*D11Mit21–D11Mit212*) carrying the MRL/MpJ-type Chr 11 (25.94–54.34 cM) (B6.MRLc11). Furthermore, by mating B6.MRLc1 mice with B6.MRLc11, we generated the double congenic mouse strain B6.MRL-(*D1Mit202–D1Mit403;D11Mit21–D11Mit212*) carrying both of the MRL/MpJ-type Chr 1 (67.97–81.63 cM) and Chr 11 (25.94–54.34 cM) (B6.MRLc1c11). Each mouse was maintained under specific pathogen-free conditions. For care and handling of experimental animals, we adhered to the Guide for the Care and Use of Laboratory Animals of Hokkaido University, Graduate School of Veterinary Medicine (approved by the Association for Assessment and Accreditation of Laboratory Animal Care International).

Experimental cryptorchidism

Adult (8- to 14-wk-old) male mice were anesthetized with an intraperitoneal injection of sodium pentobarbital (40 mg/kg body weight) dissolved in 0.01 M phosphate-buffered saline (PBS), and an abdominal incision was made. To induce unilateral cryptorchidism, the right testis was manipulated through the inguinal canal into the abdomen by cutting the gubernaculums and sutured to the abdominal wall via the fat-pad. On day 21 after the operation, both testes were removed and the weight ratio of the right cryptorchid testis to the left intact testis was calculated. Each testis was fixed overnight in Bouin’s solution and embedded in paraffin.

Heat treatment

To examine the effects of heat stress on mouse testes, 12-wk-old male mice were subjected to a single application of scrotal heat stress (SHS) of 43°C for 20 min. Briefly, after anesthesia with an intraperitoneal injection of sodium pentobarbital (40 mg/kg body weight) dissolved in 0.01 M PBS, the hind legs, tail, and scrotum containing the testes were immersed in a thermostatically controlled water bath. Untreated mice were used as controls. After 20 min, each animal was dried and returned to its cage. Mice were sacrificed at 24–72 h and 10–60 days after SHS induction to assess the short-term and long-term effects on the testes, respectively. The testes were dissected and immediately weighed. They were immersion-fixed in ice-cold 4% paraformaldehyde (PFA) in 0.1 M phosphate buffer overnight, and then embedded in paraffin.

Immunohistochemistry

The testes were then sectioned (2 µm), deparaffinized, and re-hydrated. For immunohistochemistry, sections were incubated for 15 min at 105°C in buffered citrate (pH 6.0) for antigen retrieval of the following proteins: stimulated by retinoic acid gene 8 (STRA8), DMC1 dosage suppressor of mck1 homolog, meiosis-specific homologous recombination (DMC1), SRY (sex determining region Y)-box 9 (SOX9), gremlin 2 (GREM2), and noggin

(NOG). Samples were treated with methanol containing 0.3% H_2O_2 to eliminate endogenous peroxidase. After blocking with normal serum, sections were incubated with rabbit anti-STRA8 (1:2000; Abcam, Cambridge, UK), goat anti-DMC1 (1:500; Santa Cruz Biotechnology, Santa Cruz, CA, USA), rabbit anti-single-stranded DNA (ssDNA, 1:200; IBL, Fujioka, Japan), rabbit anti-SOX9 (1:2000; Merck Millipore, Billerica, MA, USA), rabbit anti-GREM2 (1:50; Proteintech, Chicago, IL, USA), and rabbit anti-NOG (1:450; Abcam) at 4°C overnight. Next, the sections were treated with biotin-conjugated goat anti-rabbit IgG antibodies (SABPO kit; Nichirei, Tokyo, Japan) or with biotin-conjugated donkey anti-goat IgG antibodies (1:100; Santa Cruz Biotechnology) for 30 min at room temperature followed by streptavidin-peroxidase complex (SABPO kit) for 30 min at room temperature. The sections were incubated with 3,3′-diaminobenzidine tetrahydrochloride (DAB) solution containing 0.006% H_2O_2 until the stain developed and then counterstained with hematoxylin. For histological analyses, digital images of each section were acquired using a BZ-9000 microscope (Keyence, Osaka, Japan). The immunopositive cells were counted in 200–400 tubules per testis using BZ-II Analyzer software (Keyence).

Histopathology

Paraffin sections were prepared from testes fixed in either Bouin’s solution or 4% PFA, as described above, for periodic acid-Schiff-hematoxylin or von Kossa staining. For von Kossa staining, 5-μm-thick sections were incubated with 5% silver nitrate solution under direct sunlight for 60 min. The slides were then washed in water, incubated with 5% sodium thiosulfate pentahydrate for 3 min, rinsed, and counterstained for 5 min with nuclear fast red. Seminiferous tubules containing von Kossa-positive mineral deposits were counted in 200–400 tubules per testis.

Reverse transcription and quantitative real-time PCR

Total RNA was extracted from whole mouse testes using TRIzol reagent (Life Technologies). Total RNA was then treated with Turbo DNase (Life Technologies) for DNA digestion, and complementary DNA (cDNA) was synthesized via reverse transcription using ReverTra Ace (Toyobo, Osaka, Japan) and oligo-dT (Life Technologies). Quantitative real-time PCR (qPCR) analysis was performed using cDNA, gene-specific primers (Table 1), Brilliant III Ultra Fast SYBR Green qPCR Master Mix (Agilent Technologies, Santa Clara, USA), and a real-time thermal cycler (MX 3000P; Agilent Technologies). The mRNA levels of the target genes were normalized to those of actin, beta (*Actb*).

Statistical analyses

Results were expressed as the mean ± standard error (SE), and statistical analyses were performed using PASW Statistics for Windows, Version 18.0 (IBM SPSS, Chicago, IL, USA). Nonparametric Kruskal-Wallis one-way analysis of variance (ANOVA) was used to compare each strain. One-way ANOVA followed by Dunnett's test was used to compare changes between a treatment group and the corresponding untreated group or differences between C57BL/6 mice and the other strains. *P*-values less than 0.05 were considered statistically significant.

Results

The effect of continuous hyperthermia on spermatogenesis in mice

To evaluate strain-specific differences in spermatogenesis under experimental cryptorchidism, the weight ratio of the cryptorchid testis to the intact testis and their histological features were investigated at 21 days post-surgery (Fig. 1). Unlike tubules in the intact testis (Fig. 1A), germ cell loss was obvious in the cryptorchid testis of C57BL/6 mice, and the seminiferous epithelium consisted of only undifferentiated spermatogonia and Sertoli cells (Fig. 1B). In accordance with a previous report (Kon & Endoh 2001), almost all tubules in the cryptorchid testis of the MRL/MpJ mice contained numerous spermatocytes (Fig. 1C), while spermatocytes were found to a greater or lesser extent in cryptorchid testes of congenic mouse strains (Fig. 1D–F). The testicular weight ratio was significantly higher in B6.MRLc1, B6.MRLc1c11, and MRL/MpJ mice than in C57BL/6 mice. Although B6.MRLc11 mice showed a relatively higher testicular weight ratio than C57BL/6 mice, the values were significantly lower than in MRL/MpJ mice (Fig. 1G). For histological analysis, we estimated the number of remaining spermatocytes by calculating the percentage of tubule cross-sections containing spermatocytes (Fig. 1H). Each congenic strain maintained significantly higher numbers of spermatocytes than C57BL/6 mice, and B6.MRLc1c11 mice showed highest count among congenic strains. However, MRL/MpJ mice showed significantly higher heat-resistance than each congenic strain.

The effect of transient hyperthermia on spermatogenesis in mice

Figure 2 shows the absolute testis weight at multiple time points after SHS induction. Previously, we identified the locus associated with metaphase-specific apoptosis of meiotic spermatocytes on the telomeric region of MRL/MpJ-type Chr 1 (Namiki *et al.* 2003). We also reported a mutation in exonuclease 1 (*Exo1*, Chr 1, 81.90 cM), encoding a protein important for DNA repair, as a potential cause of metaphase-specific apoptosis of meiotic spermatocytes in MRL/MpJ mice (Namiki *et al.* 2003; Namiki *et al.* 2004). As we previously reported, B6.MRLc1 mice carry the MRL/MpJ-derived locus on Chr 1 responsible for metaphase-specific apoptosis (Otsuka *et al.* 2010). Because B6.MRLc1c11 mice also carry the same MRL/MpJ-derived locus, both B6.MRLc1 and B6.MRLc1c11 mice had smaller testes compared with the other strains analyzed. After SHS induction, testis weight gradually decreased over time, reaching the minimum weight 10 days after treatment in all strains. Although testis weight gradually recovered 20 days after SHS induction, it remained markedly low even at 60 days post-induction in C57BL/6, MRL/MpJ, and B6.MRLc1 mice (44.83 ± 0.01 %, 46.58 ± 0.03 %, and 41.83 ± 0.03 % compared with strain matched control groups, respectively). In contrast, B6.MRLc11 and B6.MRLc1c11 mice showed greater recovery of testis weight at 60 days after SHS induction (62.11 ± 0.02 % and 79.56 ± 0.03 % compared with strain matched control groups, respectively).

ssDNA-positive apoptotic cells, mainly spermatocytes and round spermatids, were abundant in all strains at 24 h after SHS induction, but they were rarely detected in untreated C57BL/6 controls (Fig. 3A–F). A histological analysis revealed that the number of ssDNA-positive cells peaked at 24 h after SHS induction and then decreased in all strains (Fig. 3G). Characteristically, at 24 h after SHS induction, the number of ssDNA-positive cells was significantly lower in MRL/MpJ, B6.MRLc11, and B6.MRLc1c11 mice than in C57BL/6 mice, and B6.MRLc1 mice had relatively higher numbers of apoptotic cells at 24 h and 48 h compared to the other congenic strains.

Changes in the number of primary spermatocytes at each developmental stage were examined by immunohistochemical analysis of STRA8 and DMC1 (Fig. 4 and Supplemental Fig. 1). Consistent with the induction of apoptotic germ cells as shown in Fig. 3, the number of STRA8-positive cells (preleptotene and early leptotene spermatocytes) significantly decreased beginning 24 h after SHS induction in C57BL/6 and B6.MRLc1 mice (Fig. 4A). On the other hand, STRA8-positive cells began to decrease significantly in B6.MRLc1c11 mice at 48 h and in MRL/MpJ and B6.MRLc11 mice at 72 h. C57BL/6, MRL/MpJ, and B6.MRLc1 mice maintained lower numbers of STRA8-positive cells up to 60 days after SHS induction compared to untreated controls. Consistent with the changes in testis weight, the number of STRA8-positive cells in B6.MRLc11 and B6.MRLc1c11 had recovered to normal levels at 60 days after SHS induction (Fig. 4A).

The number of DMC1-positive cells (leptotene and zygotene spermatocytes) transiently decreased in C57BL/6 mice at 24 h after SHS induction compared to untreated controls; however, the other strains did not show a similar significant decrease compared to their respective controls (Fig. 4B). Of note, DMC1-positive cells significantly increased in B6.MRLc11 and B6.MRLc1c11 mice testes until 72 h after SHS induction compared to untreated controls (Fig. 4B). However, in all strains, including B6.MRLc11 and B6.MRLc1c11, a significant loss of DMC1-positive cells was observed at 10 days after SHS induction. Similar to STRA8-positive cells, the number of DMC1-positive cells recovered to normal levels only in B6.MRLc11 and B6.MRLc1c11 mice at 60 days after SHS induction.

Mouse strain differences in the onset of testicular calcification induced by transient hyperthermia

In accordance with our previous studies, upon long-term follow-up analysis after SHS induction, C57BL/6 and MRL/MpJ mice developed remarkable testicular calcification (Fig. 5). von Kossa-positive testicular calcification initially appeared at 72 h to 10 days after SHS induction, and staining became obvious at 20 days after SHS induction in C57BL/6 and MRL/MpJ mice (Fig. 5A, B, and F). In contrast, in all congenic strains, calcified tubules were barely detectable, and partial recovery of spermatogenesis was observed at 20 days after SHS induction (Fig. 5C–F). Moreover, the onset of calcification was significantly inhibited in all congenic strains compared with C57BL/6 mice throughout the observation period. Although calcified tubules were frequently observed in MRL/MpJ mouse testis at 60 days after SHS induction, the incidence rate was significantly lower in MRL/MpJ mice than in C57BL/6 mice.

To assess damage to the seminiferous epithelium induced by SHS, the number of Sertoli cells was evaluated by immunohistochemical analysis of SOX9, a Sertoli cell marker (Fig. 6). The number of SOX9-positive cells in C57BL/6 and MRL/MpJ mice significantly decreased beginning 20 days after SHS induction, coincident with the abrupt onset of calcification (Fig. 6G). Despite the inhibition of calcification, the number of SOX9-positive cells in B6.MRLc1 mice significantly decreased at 60 days after SHS induction. Furthermore, detachment of Sertoli cells from the basement membrane was frequently observed in the tubules of C57BL/6, MRL/MpJ, and B6.MRLc1 mice at 60 days after SHS induction (Fig. 6B–D, arrows). In contrast, although some tubules in B6.MRLc11 and B6.MRLc1c11 mouse testes contained detached Sertoli cells at 60 days after SHS induction (Fig. 6E and F, arrows), the number of SOX9-positive cells significantly increased at 10 days or 10–60 days after SHS induction, respectively (Fig. 6G).

The expression of calcification-related factors in mouse testes exposed to transient heat stress

Previously, we reported that the activities of bone morphogenic protein 2 (BMP2) and GREM2, an endogenous BMP antagonist, correlated with the incidence of heat-induced testicular calcification (Chihara *et al.* 2014). Because *Grem2* localizes at 81.08 cM on murine Chr 1, we focused on *Nog*, which encodes another cytokine that inhibits the BMP2 activity and localizes at 54.34 cM on murine Chr 11 (Pardali & Ten Dijke 2012). Compared to untreated control testes, *Bmp2* mRNA expression tended to increase in testes of all strains at 10 days after

SHS induction (i.e., during early onset testicular calcification in C57BL/6 and MRL/MpJ mice) (Fig. 7A). In contrast, *Grem2* mRNA levels were significantly higher in B6.MRLc1 and B6.MRLc1c11 mice than in C57BL/6 mice at 10 days after SHS induction (Fig. 7B). Furthermore, *Nog* mRNA levels were significantly higher in MRL/MpJ, B6.MRLc11, and B6.MRLc1c11 mice than in C57BL/6 mice at 10 days after SHS induction (Fig. 7C). Notably, mRNA expression levels of *Grem2* and *Nog* were also significantly higher in the untreated testes of congenic strains carrying MRL/MpJ-derived loci on Chrs 1 and 11 compared to C57BL/6 mice (Fig. 7B and C), indicating a genetic difference in their expression.

We next analyzed the expression and localization of GREM2 and NOG proteins by immunohistochemistry at 10 days after SHS induction (Fig. 7D). Consistent with the qPCR results, GREM2 protein expression was weak in the seminiferous tubules of C57BL/6, MRL/MpJ, and B6.MRLc11 mice. In contrast, more intense GREM2 expression was observed as granular cytoplasmic aggregates in Sertoli cells of B6.MRLc1 and B6.MRLc1c11 mice at 10 days after SHS induction (Fig. 7D, arrows). Similarly, although NOG expression was weak in the seminiferous tubules of C57BL/6 and B6.MRLc1 mice, increased granular expression was detected in Sertoli cells of MRL/MpJ, B6.MRLc11, and B6.MRLc1c11 mice (Fig. 7D, arrowheads).

Discussion

Heat-shock resistant spermatogenesis under continuous hyperthermia in mice

Accumulating evidence indicates that spermatogenesis, and the development of spermatocytes and round spermatids in particular, is sensitive to hyperthermia (Blackshaw *et al.* 1973; Parvinen 1973). Interestingly, spermatocytes in MRL/MpJ mice were relatively resistant to heat stress, as previously demonstrated in experimental cryptorchidism (Kon & Endoh 2001; Kazusa *et al.* 2004). The heat stress-resistance of MRL/MpJ mouse testes is thought to depend on MRL/MpJ-type loci on Chrs 1 (81 cM region) and 11 (40 cM region) (Namiki *et al.* 2005).

In the present study, we evaluated the relative resistance to heat stress of spermatogenesis under continuous hyperthermia in B6.MRLc1, B6.MRLc11, and B6.MRLc1c11 congenic mouse strains by direct comparison to their background strains, C57BL/6 and MRL/MpJ mice. In cryptorchid testes, all MRL/MpJ-derived congenic strains maintained relatively stable spermatogenesis compared with C57BL/6 mice. It is noteworthy to mention that B6.MRLc1c11 mice, a congenic strain carrying both MRL/MpJ-type HRS loci on Chrs 1 and 11, showed significantly higher resistance to heat stress than the other two congenic strains. These results indicated that genetic interactions between MRL/MpJ-derived HRS loci on Chrs 1 and 11 may be important to maintain spermatogenesis under conditions of continuous testicular hyperthermia. However, B6.MRLc1c11 mice did not fully mimic the spermatogenic capacity of MRL/MpJ mice when subjected to continuous hyperthermia, suggesting the existence of other HRS-related loci that reside outside the 81 cM region of Chr 1 and the 40 cM region of Chr 11.

Sensitivity of spermatogenesis to transient hyperthermia in mice

In the present study, we investigated the time-dependent effects of SHS induction on spermatogenesis in C57BL/6 mice, MRL/MpJ mice, and the three additional congenic strains. Consistent with previous reports (Paul *et al.* 2008; Paul *et al.* 2009; Chihara *et al.* 2014), significant germ cell loss due to apoptosis was observed in the days following SHS induction. However, among the congenic strains, B6.MRLc11 and B6.MRLc1c11 mice inhibited apoptosis, similar to MRL/MpJ mice. Furthermore, B6.MRLc11 and B6.MRLc1c11 mice maintained a steady number of STRA8- (preleptotene and early-leptotene spermatocytes) and DMC1-positive cells (leptotene and zygotene spermatocytes) in the initial days after SHS induction. Consistent with previous findings (Chihara *et al.* 2014), neither inhibition of apoptosis nor protection of spermatogenesis against SHS induction was observed in B6.MRLc1 mice. Collectively, these results suggest that the MRL/MpJ-derived HRS locus on Chr 11 might play an important role in mitigating heat stress damage, thus maintaining spermatogenesis after transient hyperthermia.

The onset of testicular calcification after transient hyperthermia in mice

In the present study, although testicular calcification was not readily observed after experimental cryptorchidism of all strains, there were strain differences in the incidence of testicular calcification after SHS induction. These results might reflect differences in the damage induced to seminiferous epithelium between continuous and transient hyperthermia. At present, the etiology of testicular calcification is unclear. However, it has been suggested that extensive germ-cell degeneration is involved (Nistal *et al.* 1979; Vegni-Talluri *et al.* 1980; O'Shaughnessy *et al.* 2009; Kyrönlahti *et al.* 2011; Chihara *et al.* 2013; Chihara *et al.* 2014). Analysis of multiple mouse strains has shown that there may be a genetic basis for susceptibility to heat-induced testicular calcification. Both C57BL/6 and MRL/MpJ mice were suggested to have precipitating factors that led to testicular calcification (Chihara *et al.* 2014). In accordance with our previous result, B6.MRLc1 mice showed significantly decreased instances of testicular calcification after SHS induction. Thus, one of the genes that predisposes for calcification could localize on the 67.97–81.63 cM region of murine Chr 1. Previously, we identified MRL/MpJ-derived *Grem*2, which localizes at 81.08 cM on Chr 1, as a candidate factor for inhibition of calcification (Chihara *et al.* 2014). GREM2 is a cytokine that acts as an extracellular BMP antagonist (Sudo *et al.* 2004), suggesting BMP activity regulates the onset of calcification after transient scrotal hyperthermia. Indeed, many recent studies have suggested that BMP proteins play key roles in modulating not only bone calcification but also pathological calcification (e.g. vascular calcification) (Mikhaylova *et al.* 2007; Nakagawa *et al.* 2010; Pardali *et al.* 2012). Interestingly, in this study, we demonstrated that B6.MRLc11 and B6.MRLc1c11 mice showed significantly reduced testicular calcification after SHS induction. Therefore, we speculated that another BMP-relating gene may localize on the 25.94–54.34 cM region of murine Chr 11. Predictably, *Nog*, which encodes a BMP signaling inhibitor, localizes at 54.34 cM on murine Chr 11 (Pardali *et al.* 2012). After SHS induction, up-regulation and localization of GREM2 was observed in the Sertoli cells of B6.MRLc1 and B6.MRLc1c11 mice but not those of B6.MRLc11 mice. Conversely, expression on NOG was upregulated in the Sertoli cells of B6.MRLc11 and B6.MRLc1c11 mice but not in B6.MRLc1 mice. These results strongly suggest that MRL/MpJ-derived *Grem2* and *Nog* act independently as factors inhibiting calcification by antagonizing BMP activity. Further studies on the phenotype of the testis in transgenic mice overexpressing *Grem2* and *Nog* would be needed to validate this hypothesis.

Moreover, a high incidence of calcification in MRL/MpJ mouse testis suggested that MRL/MpJ mice may also have a potent precipitating factor for testicular calcification that resides outside the 67.97–81.63 cM region of Chr 1 and the 25.94–54.34 cM region of Chr 11. Indeed, the Sertoli cells of heat stress-exposed MRL/MpJ mouse testes showed degenerative changes (Fig. 6), indicating that the ability of MRL/MpJ mouse Sertoli cells to maintain spermatogenesis might be impaired long-term after SHS induction. Despite calcification inhibition, B6.MRLc1 mice showed significant Sertoli cell degeneration at 60 days after SHS induction. This result reinforced the concept that the MRL/MpJ-type HRS locus on Chr 11 is superior to the MRL/MpJ-type locus on Chr 1 in mitigating damage induced by transient hyperthermia. However, whether MRL/MpJ-derived HRS loci and calcification inhibitors are the same factors is unclear in the present study and requires further exploration.

In summary, the present study demonstrated that the cooperative effects of the MRL/MpJ-derived HRS loci on Chrs 1 and 11 are necessary to maintain spermatogenesis under continuous hyperthermia. By contrast, the MRL/MpJ-derived HRS locus on Chr 11, rather than the locus on Chr 1, might protect seminiferous epithelium from damage induced by transient hyperthermia. Based on these results, we hypothesize that MRL/MpJ-derived loci on Chrs 1 and 11 regulate testicular heat-resistance through different mechanisms. Further studies, including a more detailed analysis of the results found in the present study, may provide new insights into the mechanisms regulating testicular heat-sensitivity.

Acknowledgments

This work was supported by a Grants-in-Aid for Research fellowship from the Japan Society for the Promotion of Science (No. 24002135) and a Grants-in-Aid for Scientific Research B (No.

24380156) from the Ministry of Education, Culture, Sports, Science, and Technology of Japan.

Conflict of interest statement

The authors declare no conflict of interest.

References

Blackshaw AW, Hamilton D & Massey PF. (1973) Effect of scrotal heating on testicular enzymes and spermatogenesis in the rat. *Aust J Biol Sci* 26, 1395–1407.

Chihara M, Nakamura T, Sakakibara N, Otsuka S, Ichii O & Kon Y. (2014). The onset of heat-induced testicular calcification in mice: involvement of the telomeric locus on chromosome 1. *Am J Pathol* 184, 2480–2492.

Chihara M, Otsuka S, Ichii O & Kon Y. (2013) Vitamin A deprivation affects the progression of the spermatogenic wave and initial formation of the blood-testis barrier, resulting in irreversible testicular degeneration in mice. *J Reprod Dev* 59, 525–535.

Clark LD, Clark RK & Heber-Katz E. (1998) A new murine model for mammalian wound repair and regeneration. *Clin Immunol Immunopathol* 88, 35–45.

Garolla A, Torino M, Sartini B, Cosci I, Patassini C, Carraro U & Foresta C. (2013) Seminal and molecular evidence that sauna exposure affects human spermatogenesis. *Hum Reprod* 28, 877–885.

Guo J, Tao SX, Chen M, Shi YQ, Zhang ZQ, Li YC, Zhang XS, Hu ZY & Liu YX. (2007) Heat treatment induces liver receptor homolog-1 expression in monkey and rat Sertoli cells. *Endocrinology* 148, 1255–1265.

Ivell R. (2007) Lifestyle impact and the biology of the human scrotum. *Reprod Biol Endocrinol* 5, e15.

Kazusa K, Namiki Y, Asano A, Kon Y, Endoh D & Agui T. (2004) Differences in spermatogenesis in cryptorchid testes among various strains of mice. *Comp Med* 54, 179–184.

Kon Y. (2005) Morphogenetic investigation of metaphase-specific cell death in meiotic spermatocytes in mice. *Anat Sci Int* 80, 141–152.

Kon Y & Endoh D. (2000) Morphological study of metaphase-specific apoptosis in MRL mouse testis. *Anat Histol Embryol* 29, 313–319.

Kon Y & Endoh D. (2001) Heat-shock resistance in experimental cryptorchid testis of mice. *Mol Reprod Dev* 58, 216–222.

Kon Y, Horikoshi H & Endoh D. (1999) Metaphase-specific cell death in meiotic spermatocytes in mice. *Cell Tissue Res* 296, 359–369.

Kyrönlahti A, Euler R, Bielinska M, Schoeller EL, Moley KH, Toppari J, Heikinheimo M & Wilson DB. (2011) GATA4 regulates Sertoli cell function and fertility in adult male mice. *Mol Cell Endocrinol* 333, 85–95.

Leferovich JM, Bedelbaeva K, Samulewicz S, Zhang XM, Zwas D, Lankford EB & Heber-Katz E. (2001) Heart regeneration in adult MRL mice. *Proc Natl Acad Sci USA* 98, 9830–9835.

Li XX, Chen SR, Shen B, Yang JL, Ji SY, Wen Q, Zheng QS, Li L, Zhang J, Hu ZY, Huang XX & Liu YX. (2013) The heat-induced reversible change in the blood-testis barrier (BTB) is regulated by the androgen receptor (AR) via the partitioning-defective protein (Par) polarity complex in the mouse. *Biol Reprod* 89, 12, 1–10.

Lue YH, Hikim AP, Swerdloff RS, Im P, Taing KS, Bui T, Leung A & Wang C. (1999) Single exposure to heat induces stage-specific germ cell apoptosis in rats: role of intratesticular testosterone on stage specificity. *Endocrinology* 140, 1709–1717.

Mikhaylova L, Malmquist J & Nurminskaya M. (2007) Regulation of in vitro vascular calcification by BMP4, VEGF and Wnt3a. *Calcif Tissue Int* 81, 372–381.

Murphy ED. (1981) Lymphoproliferation (lpr) and other single-locus models for murine lupus. In: Immunologic Defects in Laboratory Animals, Vol 2 (eds M E Gershwin & B Merchant), pp. 143–173. Plenum Press, New York.

Nakagawa Y, Ikeda K, Akakabe Y, Koide M, Uraoka M, Yutaka KT, Kurimoto-Nakano R, Takahashi T, Matoba S, Yamada H, Okigaki M & Matsubara H. (2010) Paracrine osteogenic signals via bone morphogenetic protein-2 accelerate the atherosclerotic intimal calcification in vivo. *Arterioscler Thromb Vasc Biol* 30, 1908–1915.

Namiki Y, Endoh D & Kon Y. (2003) Genetic mutation associated with meiotic metaphase-specific apoptosis in MRL/MpJ mice. *Mol Reprod Dev* 64, 179–188.

Namiki Y, Kon Y, Sasaki N, Agui T & Endoh D. (2004) Exon skipping of exonuclease 1 in MRL/MpJ mice is caused by a nucleotide substitution of the branchpoint sequence in intron eight. *Jpn J Vet Res* 52, 125–134.

Namiki Y, Kon Y, Kazusa K, Asano A, Sasaki N & Agui T. (2005) Quantitative trait loci analysis of heat stress resistance of spermatocytes in the MRL/MpJ mouse. *Mamm Genome* 16, 96–102.

Nistal M, Paniagua R & Díez-Pardo JA. (1979) Testicular microlithiasis in 2 children with bilateral cryptorchidism. *J Urol* 121, 535–537.

O'Shaughnessy PJ, Monteiro A, Verhoeven G, De Gendt K & Abel MH. (2009) Occurrence of testicular microlithiasis in androgen insensitive hypogonadal mice. *Reprod Biol Endocrinol* **7**, 88.

Otsuka S, Konno A, Hashimoto Y, Sasaki N, Endoh D & Kon Y. (2008) Oocytes in newborn MRL mouse testes. *Biol Reprod* 79, 9–16.

Otsuka S, Namiki Y, Ichii O, Hashimoto Y, Sasaki N, Endoh D & Kon Y. (2010) Analysis of factors decreasing testis weight in MRL mice. *Mamm Genome* 21, 153–161.

Parvinen M. (1973) Observations on freshly isolated and accurately identified spermatogenic cells of the rat. Early effects of heat and short-time experimental cryptorchidism. *Virchows Arch B Cell Pathol* 13, 38–47.

Paul C, Murray AA, Spears N & Saunders PT. (2008) A single, mild, transient scrotal heat stress causes DNA damage, subfertility and impairs formation of blastocysts in mice. *Reproduction* 136, 73–84.

Paul C, Teng S & Saunders PT. (2009) A single, mild, transient scrotal heat stress causes hypoxia and oxidative stress in mouse testes, which induces germ cell death. *Biol Reprod* 80, 913–919.

Pardali E & ten Dijke P. (2012) TGFβ signaling and cardiovascular diseases. *Int J Biol Sci* 8, 195–213.

Rockett JC, Mapp FL, Garges JB, Luft JC, Mori C & Dix DJ. (2001) Effects of hyperthermia on spermatogenesis, apoptosis, gene expression, and fertility in adult male mice. *Biol Reprod* 65, 229–239.

Steinberger A. (1991) Effects of temperature on the biochemistry of the testis. *Adv Exp Med Biol* 286, 33–47.

Sudo S, Avsian-Kretchmer O, Wang LS & Hsueh AJ. (2004) Protein related to DAN and cerberus is a bone morphogenetic protein antagonist that participates in ovarian paracrine regulation. *J Biol Chem* 279, 23134–23141.

Vegni-Talluri M, Bigliardi E, Vanni MG & Tota G. (1980) Testicular microliths: their origin and structure. *J Urol* 124, 105–107.

Yin Y, Hawkins KL, DeWolf WC & Morgentaler A. (1997) Heat stress causes testicular germ cell apoptosis in adult mice. *J Androl* 18, 159–165.

Figure legends

Fig. 1. Heat-shock resistance in experimental cryptorchid testis of mice.

(A–F) Periodic acid-Schiff-hematoxylin stained cross sections of testes from mice at 21 days after the cryptorchidism operation. No histological abnormalities were observed in intact C57BL/6 mouse testis (A). In the cryptorchid testis of C57BL/6 mice, germ cell are largely absent, while Sertoli cells and undifferentiated spermatogonia survived (B). Germ cells, with the exception of spermatids, were observed in the cryptorchid testis of MRL/MpJ mice (C). In the cryptorchid testes of B6.MRLc1 (D), B6.MRLc11 (E), and B6.MRLc1c11 (F) mice, spermatocytes survived in some seminiferous tubules. Scale bars = 50 μm. (G) Cryptorchid to intact testis weight ratio at 21 days after the cryptorchidism operation ($n \geq 5$). Values shown are the mean ± SE. *$P < 0.05$ versus another strain, non-parametric one-way ANOVA (Kruskal-Wallis). (H) Incidence of seminiferous tubules containing spermatocytes at 21 days after cryptorchidism operation. Tubules containing at least one spermatocyte were counted in 200–500 tubules per testis ($n \geq 5$). Values shown are the mean ± SE. *$P < 0.05$ versus another strain, non-parametric one-way ANOVA (Kruskal-Wallis).

Fig. 2. Changes in testicular weight after induction of scrotal heat stress.

Control, untreated control; h, hours after scrotal heat stress (SHS) induction; d, days after SHS induction. $n \geq 3$. Values shown are the mean ± SE.

Fig. 3. Apoptosis in mouse testes after scrotal heat stress induction.

(A–F) Appearance of ssDNA-positive cells in the seminiferous epithelium after scrotal heat stress (SHS) induction. ssDNA-positive cells were infrequently detected in testes from untreated C57BL/6 mice (A). At 24 h after SHS induction, large portions of seminiferous tubules from C57BL/6 (B) and B6.MRLc1 (D) mice contained numerous ssDNA-positive cells, whereas testes of MRL/MpJ (C), B6.MRLc11 (E), and B6.MRLc1c11 (F) mice contained fewer apoptotic cells. Scale bars = 50 µm. (G) Changes in the number of apoptotic cells in C57BL/6, MRL/MpJ, B6.MRLc1, B6.MRLc11, and B6.MRLc1c11 mice after SHS induction. The total number of ssDNA-positive cells was counted in 200–400 tubules per control testis and heat shock-exposed testis ($n \geq 3$). h, hours after SHS induction; d, days after SHS induction. Values shown are the mean ± SE. *$P < 0.05$ versus C57BL/6 mice at the same time point, as determined by one-way ANOVA followed by Dunnett's test.

Fig. 4. The changes in spermatocyte composition in mouse testes after scrotal heat stress induction.

The changes in the numbers of STRA8-positive cells (A) and DMC1-positive cells (B) in the testes of each mouse strain after scrotal heat stress (SHS) induction. Positive cells were counted in 200–400 tubules per testis ($n \geq 3$). h, hours after SHS induction; d, days after SHS induction. Values shown are the mean ± SE. *$P < 0.05$ versus strain-matched controls, as determined by one-way ANOVA followed by Dunnett’s test.

Fig. 5. The onset of calcification in mouse testes after scrotal heat stress induction.

(A–E) von Kossa-stained cross sections of testes from C57BL/6 (A), MRL/MpJ (B), B6.MRLc1 (C), B6.MRLc11 (D), and B6.MRLc1c11 (E) mice at 20 days after scrotal heat stress (SHS) induction. Most tubules in C57BL/6 and MRL/MpJ mice contained von Kossa-positive granules (black), whereas granules were barely detectable in the testis of B6.MRLc1, B6.MRLc11, and B6.MRLc1c11 mice. Scale bars = 50 µm. (F) Changes in the incidence of von Kossa-positive seminiferous tubules in testes from each strain after SHS induction. Seminiferous tubules containing von Kossa-positive mineral deposits were counted in 200–400 tubules per testis ($n \geq 3$). h, hours after SHS induction; d, days after SHS induction. Values shown are the mean ± SE. *$P < 0.05$ versus C57BL/6 mice at the same time point, one-way ANOVA followed by Dunnett’s test.

Fig. 6. Damage to Sertoli cells in mouse testes after scrotal heat stress induction.

(A–F) Appearance of SOX9-positive cells in the seminiferous epithelium after scrotal heat stress (SHS) induction. SOX9-positive cells were aligned along the basement membrane of seminiferous tubules in untreated C57BL/6 mouse testes (A). At 60 days after SHS induction, SOX9-positive cell detachment from the basement membrane (arrows) was concomitant with a significant decrease in these cells was observed in tubules from C57BL/6 (B), MRL/MpJ (C), and B6.MRLc1 (D) mice. Although detached, SOX9-positive cells (arrows) were observed in some tubules from B6.MRLc11 (E) and B6.MRLc1c11 (F) mice at 60 days after SHS induction; however, most SOX9-positive cells were aligned along the basement membrane of tubules. Scale bars = 50 µm. (G) Changes in the number of SOX9-positive cells in the testes of each mouse strain after SHS induction. Positive cells were counted in 200–400 tubules, including calcified tubules, per testis ($n \geq 3$). h, hours after SHS induction; d, days after SHS induction.. Values shown are the mean ± SE. *$P < 0.05$ versus strain-matched controls, as determined by one-way ANOVA followed by Dunnett's test.

Fig. 7. Expression of candidate calcification-regulatory molecules in mouse testes after scrotal heat stress induction.

(A–C) qPCR results indicating changes in *Bmp2* (A), *Grem2* (B), and *Nog* (C) mRNA levels in the testes of each mouse strain after scrotal heat stress (SHS) induction ($n \geq 3$). d, days after SHS induction.. Values shown are the mean ± SE. **P* < 0.05 versus C57BL/6 mice at the same time point; one-way ANOVA followed by Dunnett's test. (D) Immunohistochemical analysis of GREM2 and NOG proteins in the testes of C57BL/6, MRL/MpJ, B6.MRLc1, B6.MRLc11, and B6.MRLc1c11 mice at 10 days after SHS induction. GREM2 proteins were identified as granular cytoplasmic aggregates in the Sertoli cells of the B6.MRLc1 and B6.MRLc1c11 testes (arrows), whereas immunopositivity of GREM2 was weak in C57BL/6, MRL/MpJ, and B6.MRLc11 mice. Similarly, NOG proteins were found as granular cytoplasmic aggregates in the Sertoli cells of MRL/MpJ, B6.MRLc11, and B6.MRLc1c11 mice (arrowheads), whereas the immunopositivity of NOG was weak in C57BL/6 and B6.MRLc1 mice. Scale bars = 10 μm.

Supplemental Figure Legend

Supplemental Figure 1. Appearance of spermatocytes at various meiotic stages in mouse testes after scrotal heat stress induction.

(A–F) The appearance of STRA8-positive cells in the seminiferous tubules. Cells positive for STRA8 (preleptotene and early leptotene spermatocytes) were observed in a seminiferous epithelial cycle-specific manner in untreated control testis from C57BL/6 mice (A). At 48 h after scrotal heat stress (SHS) induction, STRA8-positive cells were barely detectable in C57BL/6 (B) and B6.MRLc1 (D) mice, whereas they were abundantly present in MRL/MpJ (C), B6.MRLc11 (E), and B6.MRLc1c11 mice (F). (G–L) The appearance of DMC1-positive cells (leptotene and zygotene spermatocytes) in the seminiferous tubules. Tubules of testis from untreated control C57BL/6 mice contained DMC1-positive cells in a cycle-dependent manner (G). At 24 h after SHS induction, the number of DMC1-positive cells decreased, and DCM1 positivity weakened in C57BL/6 (H) and B6.MRLc1 (J) mice. In contrast, MRL/MpJ (I), B6.MRLc11 (K), and B6.MRLc1c11 (L) mice maintained DMC1-positive cells. Scale bars = 50 µm.

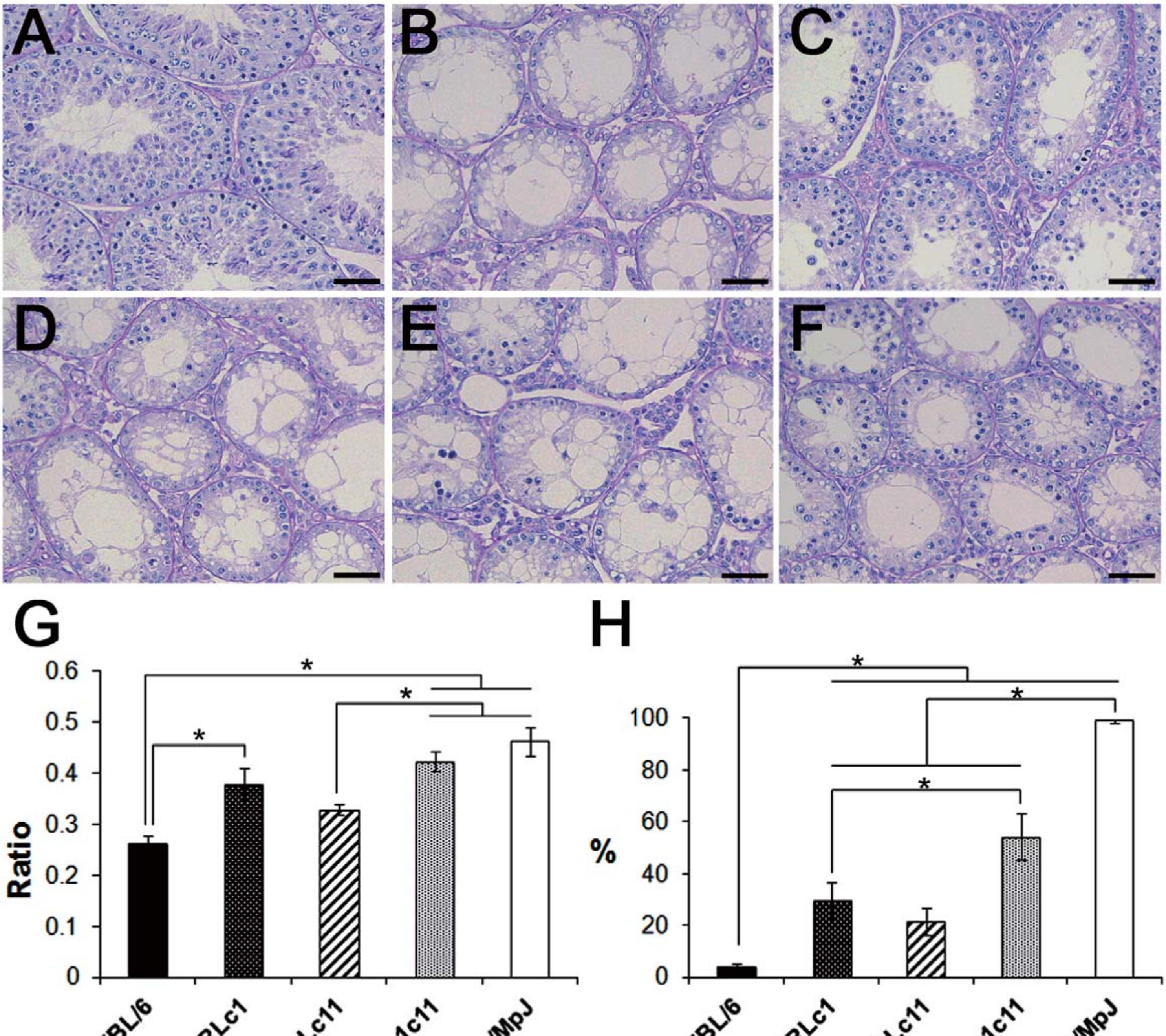
A
B
C
D
E
F
G
Ratio
0.6
0.5
0.4
0.3
0.2
0.1
0
*
*
*
C57BL/6
B6.MRLc1
B6.MRLc11
B6.MRLc1c11
MRL/MpJ
H
%
100
80
60
40
20
0
*
*
*
C57BL/6
B6.MRLc1
B6.MRLc11
B6.MRLc1c11
MRL/MpJ

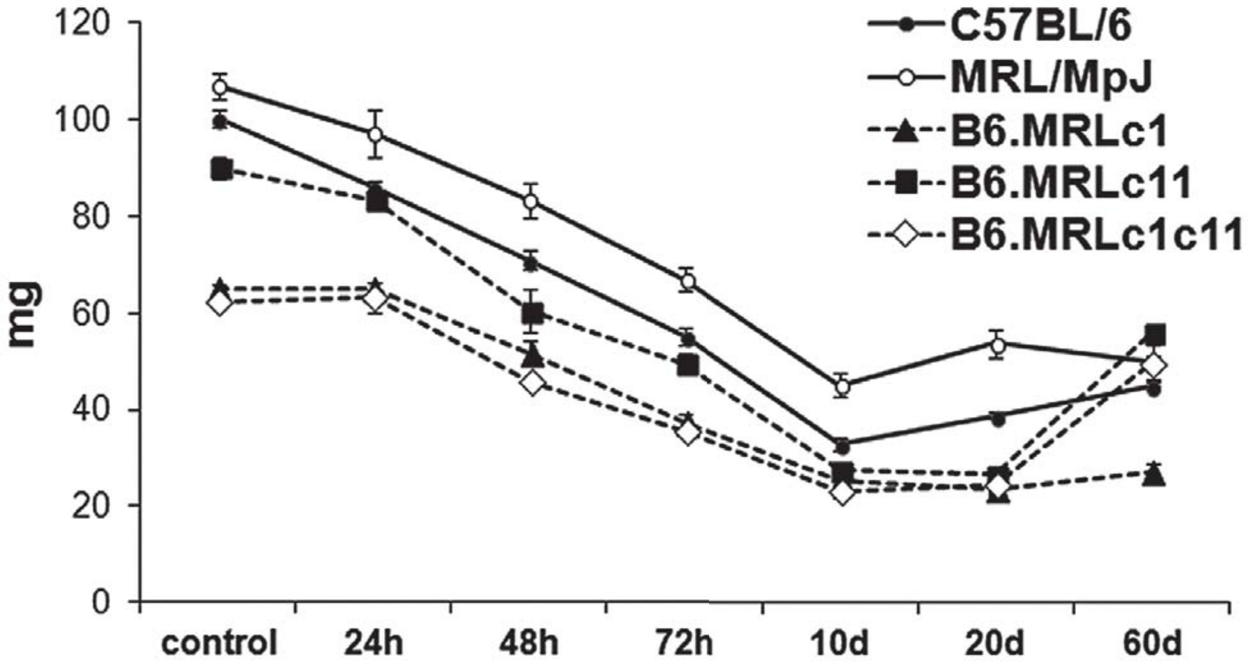

C57BL/6
MRL/MpJ
B6.MRLc1
B6.MRLc11
B6.MRLc1c11
mg
120
100
80
60
40
20
0
control
24h
48h
72h
10d
20d
60d

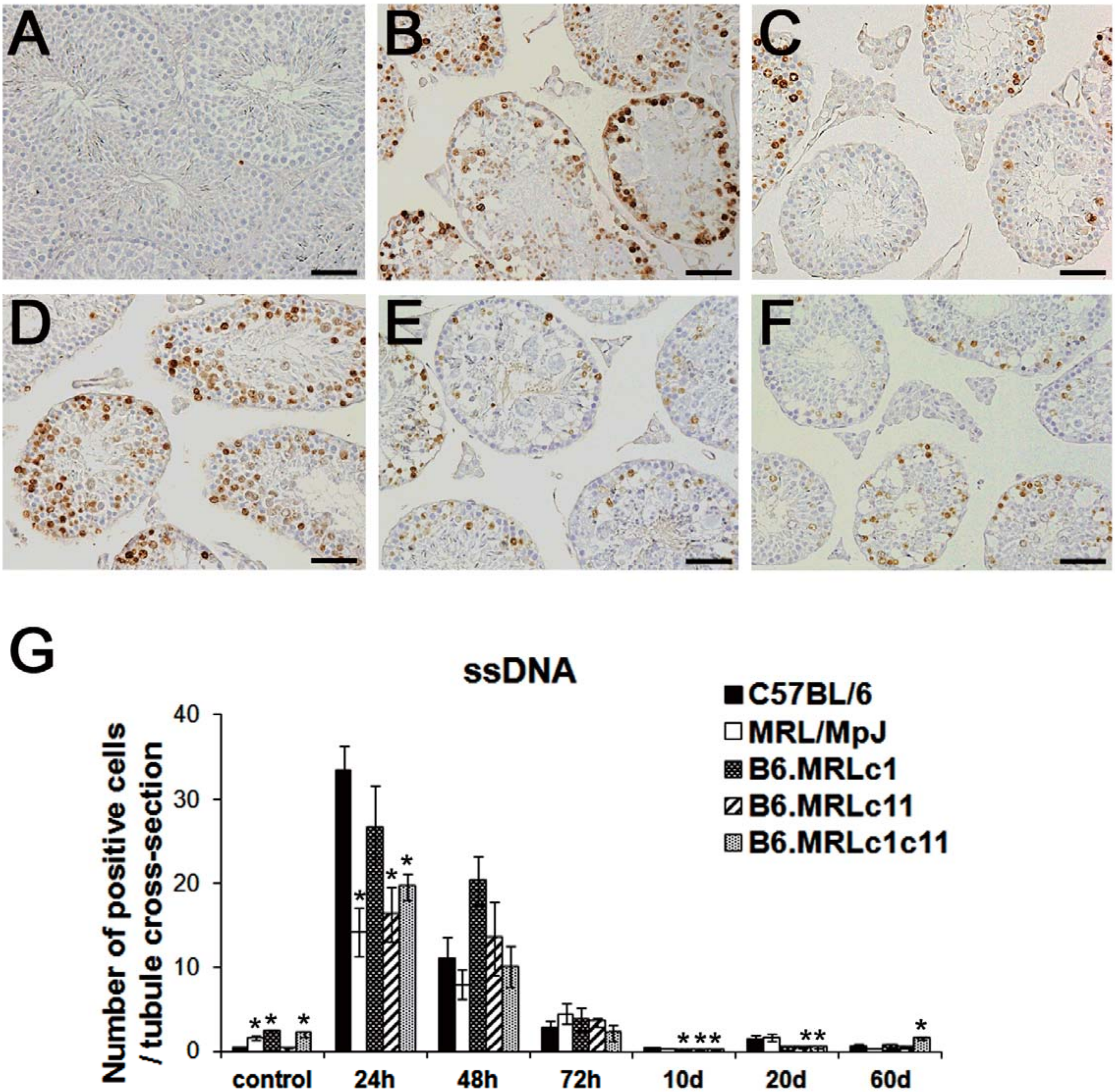
A
B
C
D
E
F
G
ssDNA
C57BL/6
MRL/MpJ
B6.MRLc1
B6.MRLc11
B6.MRLc1c11
Number of positive cells
/tubule cross-section
0
10
20
30
40
control
24h
48h
72h
10d
20d
60d

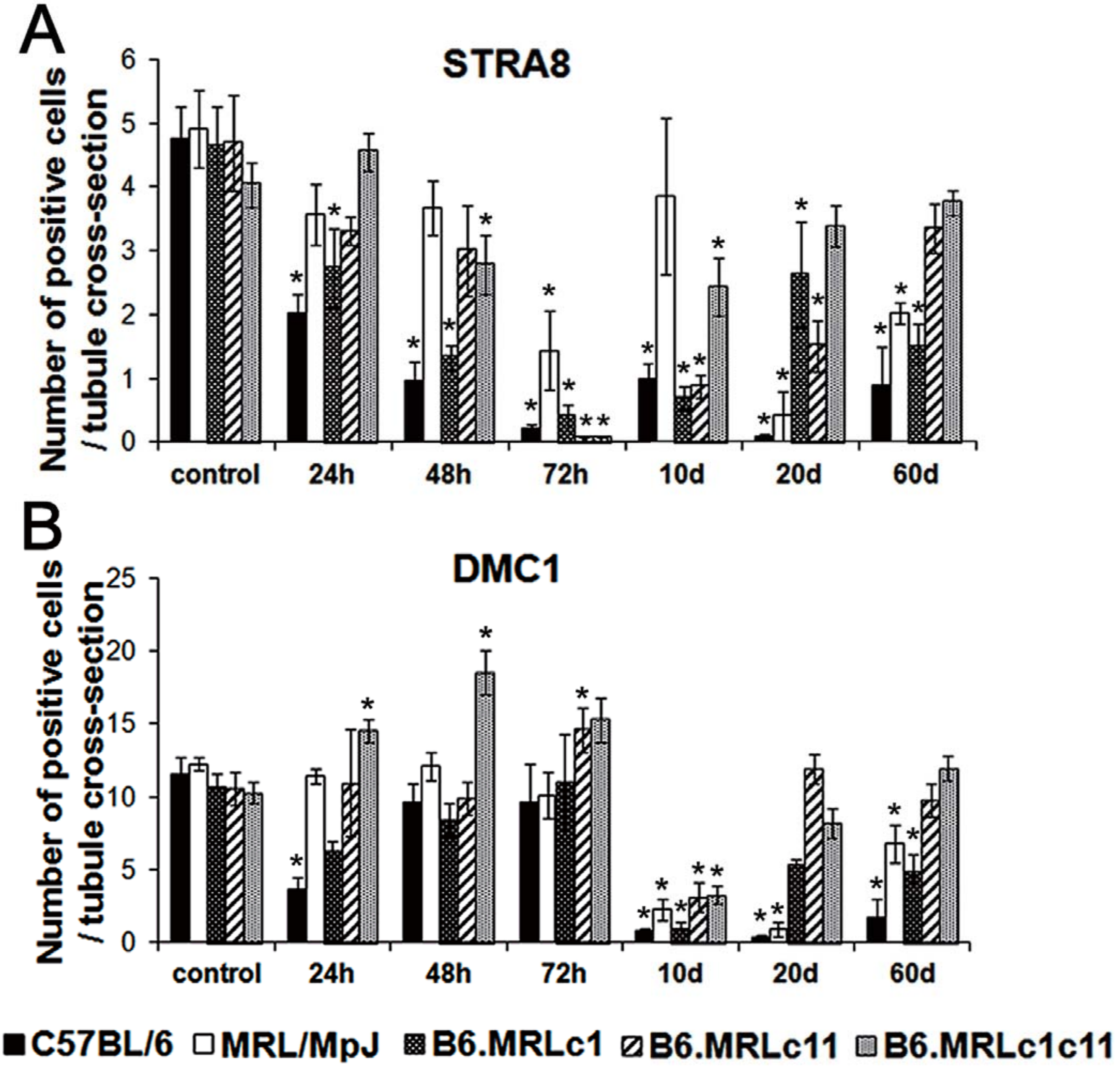
A
STRA8
Number of positive cells / tubule cross-section
0
1
2
3
4
5
6
control
24h
48h
72h
10d
20d
60d
B
DMC1
Number of positive cells / tubule cross-section
0
5
10
15
20
25
control
24h
48h
72h
10d
20d
60d
C57BL/6
MRL/MpJ
B6.MRLc1
B6.MRLc11
B6.MRLc1c11

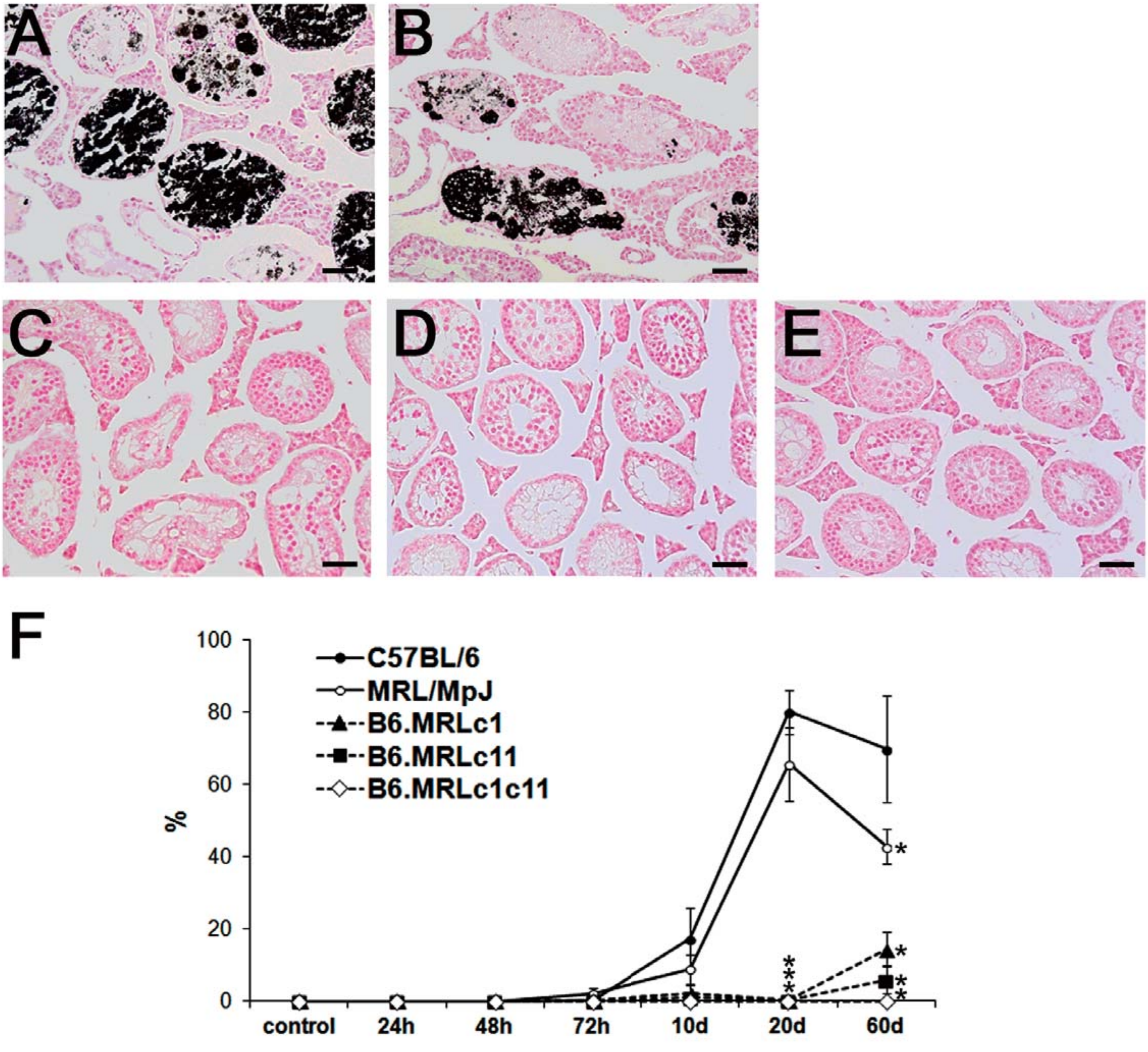
A
B
C
D
E
F
C57BL/6
MRL/MpJ
B6.MRLc1
B6.MRLc11
B6.MRLc1c11
%
100
80
60
40
20
0
control
24h
48h
72h
10d
20d
60d
*

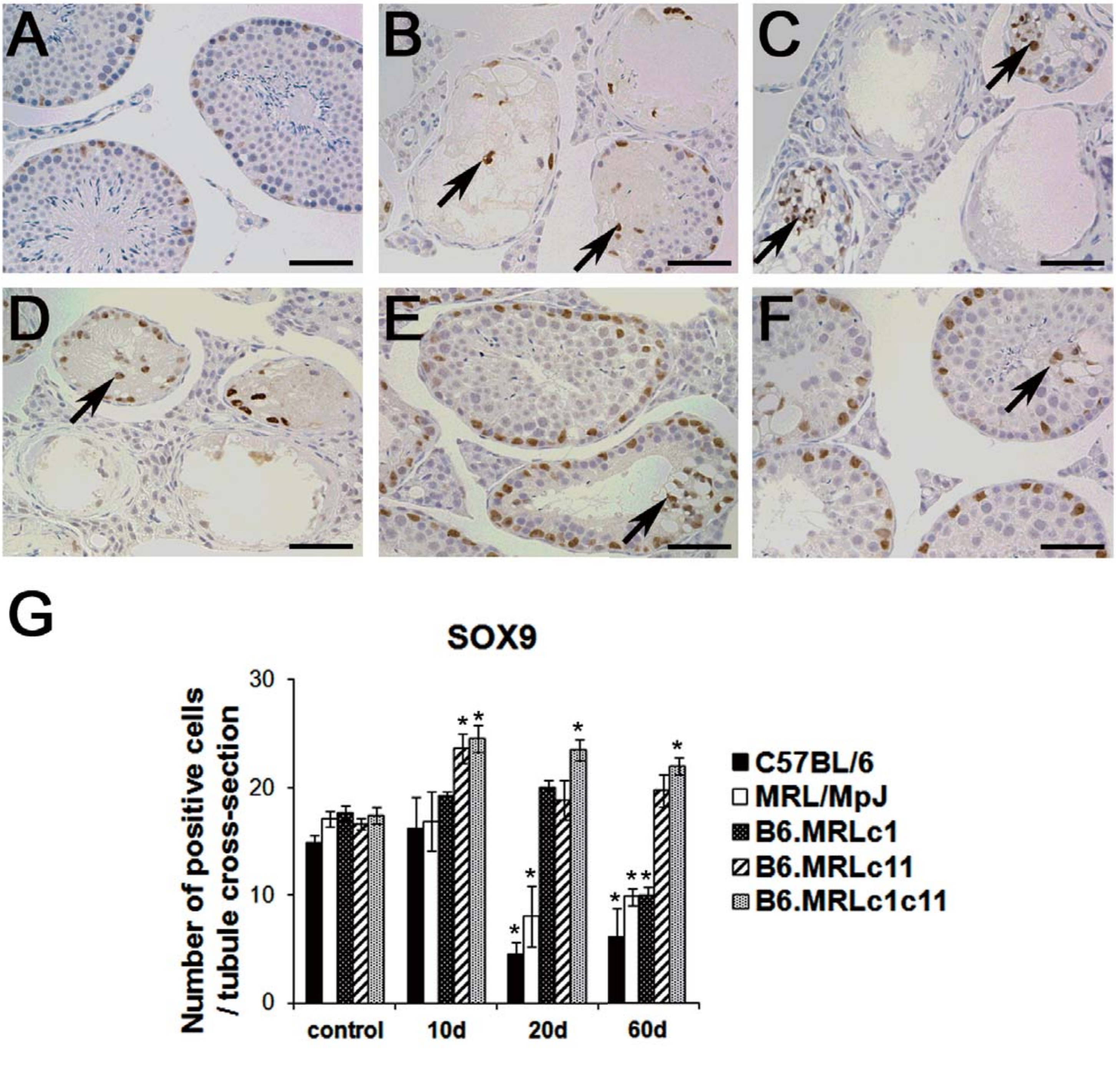

A
B
C
D
E
F
G
SOX9
Number of positive cells / tubule cross-section
30
20
10
0
control
10d
20d
60d
C57BL/6
MRL/MpJ
B6.MRLc1
B6.MRLc11
B6.MRLc1c11

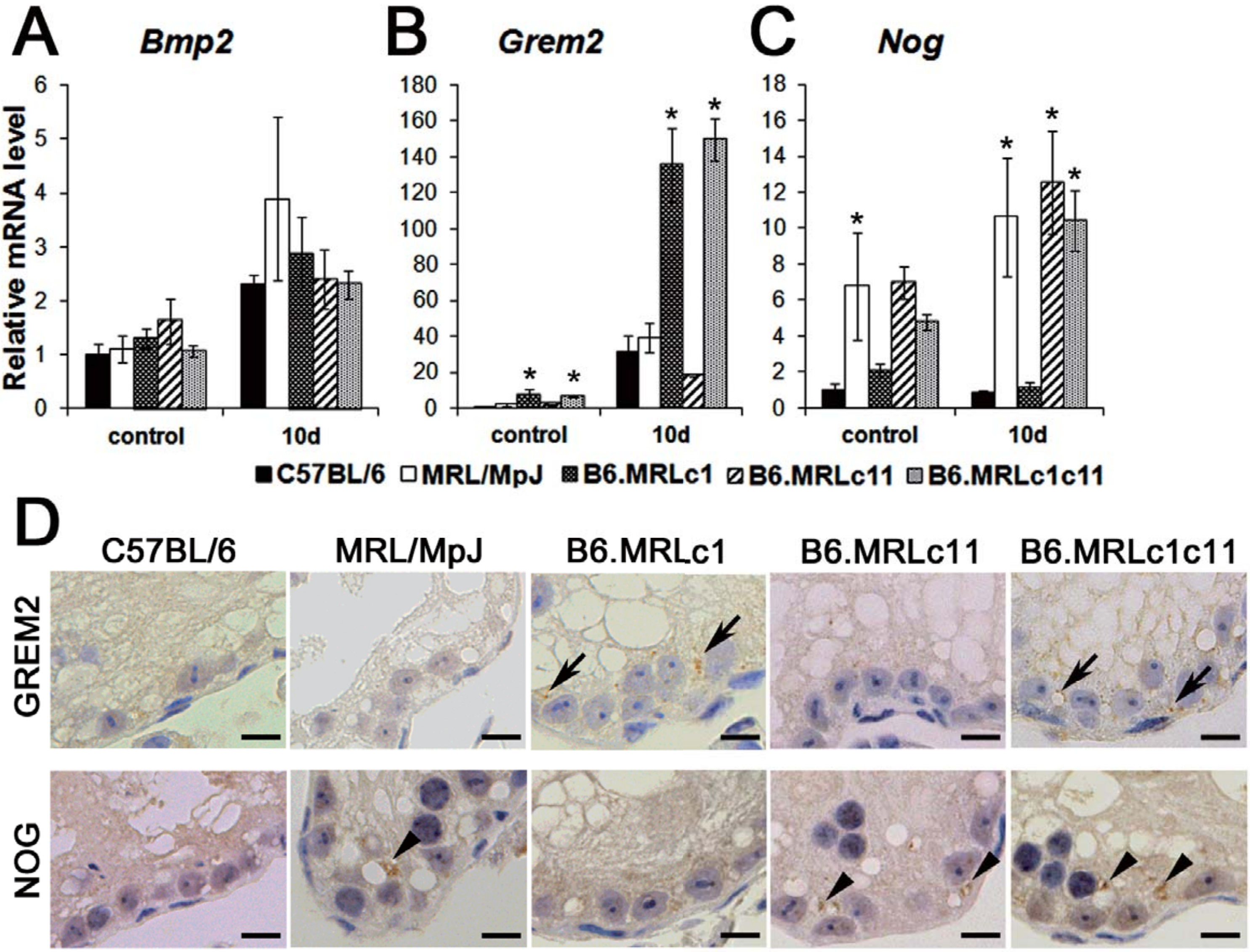

A
Bmp2
B
Grem2
C
Nog
Relative mRNA level
control
10d
C57BL/6
MRL/MpJ
B6.MRLc1
B6.MRLc11
B6.MRLc1c11
D
GREM2
NOG